J. Adv. Model. Earth Syst., **Vol. 1**, Art. #14, 13 pp.

Sensitivity of Land-Atmosphere Exchanges to Overshooting PBL Thermals in an Idealized Coupled Model

Erica L. McGrath-Spangler, A. Scott Denning, Katherine D. Corbin and Ian T. Baker

Department of Atmospheric Science, Colorado State University, Fort Collins, Colorado, USA

Manuscript submitted 4 November 2008; in final form 23 October 2009

The response of atmospheric carbon dioxide to a given amount of surface flux is inversely proportional to the depth of the planetary boundary layer (PBL). Overshooting thermals that entrain free tropospheric air down into the boundary layer modify the characteristics and depth of the mixed layer through the insertion of energy and mass. In addition, entrainment "dilutes" the effects of surface fluxes on scalar quantities (temperature, water vapor, carbon dioxide, etc.) in the PBL. Therefore, incorrect simulation of PBL depth can lead to linear errors in estimates of carbon dioxide fluxes in inverse models. Dilution by entrainment directly alters the surface-air gradients in scalar properties, which serve as the "driving force" for surface fluxes. In addition, changes in near-surface temperature and water vapor affect surface fluxes through physiological processes in plant canopies (e.g. stomatal conductance). Although overshooting thermals are important in the physical world, their effects are unresolved in most regional models. We explore the sensitivity of surface fluxes and PBL scalars to the intensity of PBL top entrainment by manipulating its strength in an idealized version of the coupled SiB-RAMS model. An entrainment parameterization based on the virtual potential temperature flux at the surface is implemented into SiB-RAMS to produce a warmer and drier mixed layer, to alter the surface fluxes, and to increase the depth of the PBL. These variations produce modified CO_2 concentrations and vary with the strength of the parameterized entrainment.

DOI:10.3894/JAMES.2009.1.14

1. Introduction

The planetary boundary layer depth (Z_i) is important for carbon budget studies. Carbon dioxide (CO_2) is released and absorbed by land ecosystems on a daily and seasonal basis. The amount of uptake and release of carbon by plants is diluted through the volume of the boundary layer so that the concentration of carbon dioxide within the boundary layer is dependent upon the PBL height (Denning et al. 1995; Yi et al. 2001, 2004). The PBL to which we refer is also described as the mixed layer or the boundary layer. We will refer to the PBL and the boundary layer interchangeably.

Atmospheric inversions are a useful method for estimating surface sources and sinks of CO_2 (e.g. Gurney et al. 2002; Gerbig et al. 2003a; Zupanski et al. 2007). Downstream tracer concentrations are compared to observations and used to optimize prior upstream sources and sinks (Gerbig et al. 2003b; Zupanski et al. 2007). In this manner, model fluxes of CO_2 are corrected with observations. The sensitivity of tracer concentrations to surface fluxes is inversely proportional to the depth of the boundary layer, so errors in Z_i translate linearly to errors in retrieved fluxes (Denning et al. 1995, 1996b, 1999, 2008; Zhang 2002; Gerbig et al. 2003a, 2008). These errors can lead to the inaccurate estimation of carbon sources and sinks.

During the daytime, in the clear atmosphere, the surface heats up through absorption of solar radiation producing a statically unstable temperature profile. This warm surface air is positively buoyant and rises through the mixed layer in warm air plumes or thermals. Due to their momentum, rising thermals overshoot their neutral level and continue into the overlying inversion layer, becoming negatively buoyant. These thermals fall back down into the mixed layer, bringing with them warm, dry free tropospheric air that is then entrained into the boundary layer by turbulent eddies (Stull 1976, 1988; Sullivan et al. 1998).

The boundary layer is the volume through which surface CO_2 exchange occurs. As this layer deepens, the effect of carbon assimilation is diluted through a greater volume. This means that for equal rates of assimilation, a deeper boundary layer exhibits a smaller decrease in the concentration of carbon (Denning et al. 1995; Yi et al. 2001, 2004;

To whom correspondence should be addressed.
Erica L. McGrath-Spangler, Department of Atmospheric Science, Colorado State University, Fort Collins, CO 80523-1371, USA
emcgrath@atmos.colostate.edu

Gerbig et al. 2008). The temperature and humidity conditions of the boundary layer not only affect the energy budget of the layer, but also the physiological state of the vegetation. As temperatures increase and humidity decreases, the plants can begin to show signs of stress (Davis et al. 1997). This decreases the assimilation of carbon and higher soil temperatures increase heterotrophic respiration. All of these effects combine to modify CO_2 concentrations near the surface. The importance of including the effects of overshooting thermals in modeling studies thus becomes apparent if the concentration of carbon in the boundary layer or the behavior of the surface vegetation is vital to the study.

Mesoscale meteorological modeling usually uses a resolution too coarse to resolve even the largest overshooting thermals and thus does not capture the entrainment process at the top of the boundary layer (Ayotte et al. 1996; Gerbig et al. 2003a); consequently, these models must include a parameterization of entrainment (André et al. 1978). The horizontal scale of boundary layer thermals is about $1.5 * Z_i$ or on the scale of 100 meters to two kilometers (Stull 1988). According to Pielke (1991), at least four grid increments are required to represent an atmospheric feature reasonably. This means that, at best, the horizontal grid increment of the mesoscale model would need to be 500 meters and sometimes as fine as twenty-five meters. Even finer grid increments would be needed in order to resolve the mixing across the inversion. Currently, model simulations with this resolution are too computationally expensive for large model domains and over long periods of time and cannot be done to fully resolve boundary layer thermals.

Since one of the most important roles of any model is to represent boundary layer top entrainment (Ayotte et al. 1996), several attempts have been made to understand entrainment better through large eddy simulations (LES) (Sullivan et al. 1998; Stevens and Bretherton 1999) and through laboratory experiments (Sayler and Breidenthal 1998). These studies conclude that overshooting thermals play a crucial role in entrainment mechanics and that the strength of entrainment varies with atmospheric conditions. Unfortunately, atmospheric observations of entrainment rates are difficult because of mesoscale variations and coupling between physical processes (Davis et al. 1997; Sullivan et al. 1998; Cohn and Angevine 2000).

Beljaars and Betts (1992) used the European Centre for Medium-Range Weather Forecasts (ECMWF) model in their simulations of the boundary layer. They found in their August simulations over the Konza prairie during the First ISLSCP (International Satellite Land Surface Climatology Project) Field Experiment (FIFE) that the model produced boundary layer conditions that were too cool and too moist and that this boundary layer grew too slowly. They suggested that this was due to the lack of entrainment in their model. The ECMWF model, like SiB-RAMS, grew the PBL through encroachment as the surface warmed, rather than through explicit PBL top entrainment. After including an entrainment parameterization, their results improved.

In the current formulation of the Brazilian version of the Regional Atmospheric Modeling System (BRAMS) version 2.0, boundary layer top entrainment is implicitly included as layer by layer mixing and is not adequate to represent the mixing associated with overshooting thermals (Freitas et al. 2006). The boundary layer depth is diagnosed from the virtual potential temperature profile by finding the lowest layer where the virtual potential temperature profile increases by a specified amount (0.5 K in these simulations), indicating the capping inversion.

In RAMS, the vertical eddy diffusivities for momentum, heat, and TKE are inversely proportional to the vertical gradient of potential temperature through an equation for the turbulent length scale for stable conditions by André et al. (1978). They admit that this parameterization is crude and not elaborate enough to describe the turbulence in a strongly thermally stratified environment. As the stratification increases, the turbulent length scale and the vertical eddy diffusivities decrease, increasing the TKE eddy dissipation term, and can do so enough to prevent vertical mixing. The temperature inversion at the top of the boundary layer can then act similar to a material surface and retard the exchange of energy and mass that occurs in the physical world. The PBL in RAMS grows by encroachment as the surface warms, but there is no explicit representation of PBL top entrainment. If the simulated boundary layer is too cold, too moist, and too shallow when compared to observations, such as was found by Beljaars and Betts (1992), an entrainment parameterization can produce better results by improving the interactions between entrainment and the surface fluxes.

This paper discusses the sensitivity of the response of the land surface to enhanced entrainment at the top of the PBL that warms, dries, and increases the depth of the boundary layer. The parameterization includes a tunable coefficient that is allowed to vary in the different simulations, and comparisons are presented that show the effects of changing this coefficient. This parameterization has been studied by numerous authors including Betts (1973), Carson (1973), Deardorff (1974), Rayment and Readings (1974), Willis and Deardorff (1974), Stull (1976), Davis et al. (1997), Sullivan et al. (1998), and Yi et al. (2001) and this paper seeks to understand the interaction with the surface and the subsequent effects on the mixed layer. Section 2 is a description of the model setup. Section 3 discusses the parameterization itself and its implementation into RAMS. Results of idealized model simulations using the parameterization are given in section 4. A conclusion and direction for future work is presented in section 5.

2. Model setup

The parameterization has been implemented in a modified form of RAMS version 5.04 called BRAMS version 2.0. The

major differences between RAMS and BRAMS are the implementation of the Grell convection scheme and the shallow convection scheme (Walko et al. 2002). The surface model used is the third version of the Simple Biosphere Model (SiB3), initially developed by Sellers et al. (1986). The coupling of the surface model and atmospheric model is called SiB-RAMS (Denning et al. 2003; Nicholls et al. 2004; Wang et al. 2007; Corbin et al. 2008).

RAMS was initially developed at Colorado State University as a non-hydrostatic three-dimensional model in order to study mesoscale and cloud-scale phenomena (Pielke 1974; Tripoli and Cotton 1982; Pielke et al. 1992; Cotton et al. 2003). It includes time-dependent equations for velocity, ice-liquid water potential temperature, total water mixing ratio and diagnostic formulations of potential temperature and vapor mixing ratio (Denning et al. 2003) on either a terrain-following σ_z coordinate system or the Adaptive Aperature (ADAP) coordinate system. The ADAP coordinate is a fully Cartesian grid in which the grid cells are allowed to intersect the topography and allows partial grid cells along the topography (Walko et al. 2002). The terrain-following coordinate system is used in the simulations discussed in this paper, but the implemented parameterization accommodates both systems.

Plant and plant photosynthesis are parameterized in the SiB model in an attempt to mimic the real world. SiB is a land-surface parameterization used to compute biophysical exchanges in climate models (Sellers et al. 1986), but also includes ecosystem metabolism (Sellers et al. 1996; Denning et al. 1996a). Farquhar et al. (1980) originally developed the photosynthesis parameterization. SiB is an interactive dynamic land surface model that determines the surface boundary condition to RAMS.

A single grid was used on a domain of 200 km × 200 km with 25 individual grid cells (5 × 5) with a size of 40 km × 40 km each, centered at 45°N and 90°W. This grid spacing allows the resolution of mesoscale features, but is much too coarse to resolve the individual thermals that entrain free atmospheric air into the boundary layer. Sixty-five vertical grid levels were used with the lowest level at about 30 m and extending up to a domain top of 12.8 km with a vertical grid stretch ratio of roughly 1.1. Increased vertical resolution was included near common boundary layer depth in order to resolve variations in the effects of the parameterization due to varying values of the tunable parameter.

Cyclic boundary conditions were used to isolate local processes that control PBL depth. Since the domain was periodic, large-scale advective influences were not included. The domain characteristics were horizontally homogeneous so that there were no influences from surface heterogeneity and no weather systems were allowed to advect into the domain. The only acting forces were those associated with the diurnal cycle and the parameterization itself. This setup also allowed the runs to be computationally inexpensive and quick to run. The simulation was allowed to run for 72 hours, in addition to a one week spin up. The emphasis of this setup was to produce a simplified and idealized case in order to isolate the effects of the entrainment parameterization. It therefore does not resemble any particular event and model responses should be considered in this context.

The vertical profiles of pressure, temperature, humidity, and wind velocity were initialized horizontally homogeneously from a relatively cool August sounding, typical of Green Bay, Wisconsin at 44.48°N and 88.13°W with winds predominately out of the west and northwest. The topography was defined as flat and at sea level everywhere in the domain, removing any effects of terrain on boundary layer depth or growth. Similarly, the vegetation, soil textural class, fraction of photosynthetically active radiation (FPAR), and leaf area index (LAI) were all prescribed as horizontally homogeneous. The vegetation type was C3 tall broadleaf and needleleaf trees while the soil type was loam. The default FPAR and LAI used were 0.93 and 6.2, respectively. In order to isolate the effects of dry convection, all water present in the model had to remain as water vapor, even if supersaturation occurred, in order to prevent the formation of clouds and precipitation in order to simplify the problem. The turbulence closure option used during these simulations was the Mellor and Yamada (1982) scheme for vertical diffusion. Mellor and Yamada is a local option that employs a prognostic turbulent kinetic energy.

3. Entrainment parameterization and implementation

During the growing season, at the inversion interface, overshooting thermals inject cool, moist, CO_2-depleted turbulent boundary layer air into the overlying inversion and entrain warm, CO_2-rich free tropospheric air downward creating negative heat and carbon fluxes in the region of overshoot. The profile of heat flux throughout the well-mixed, quasi-steady boundary layer is often approximated as linear (Stull 1976). Above the inversion, the perturbation vertical velocity is assumed zero, implying the heat flux is also zero.

This implies that the negative heat flux at the base of the capping inversion ($\overline{w'\theta_v'}|_{zi}$) is linearly proportional to the heat flux at the surface, leading to the closure assumption for the heat flux at the top of the boundary layer:

$$\overline{w'\theta_v'}|_{zi} = -\alpha \overline{w'\theta_v'}|_s \tag{1}$$

where α is the proportionality constant (Stull 1988). Estimates of α from experimentation and theory range anywhere from zero to one with most published values being between 0.1 and 0.3 (e.g. Betts 1973; Carson 1973; Deardorff 1974; Rayment and Readings 1974; Willis and Deardorff 1974; Stull 1976; Davis et al. 1997; Sullivan et al. 1998; Yi et al. 2001).

The assumption that the heat flux at the top of the boundary layer is negatively proportional to the surface heat flux was used to include fluxes of multiple variables from

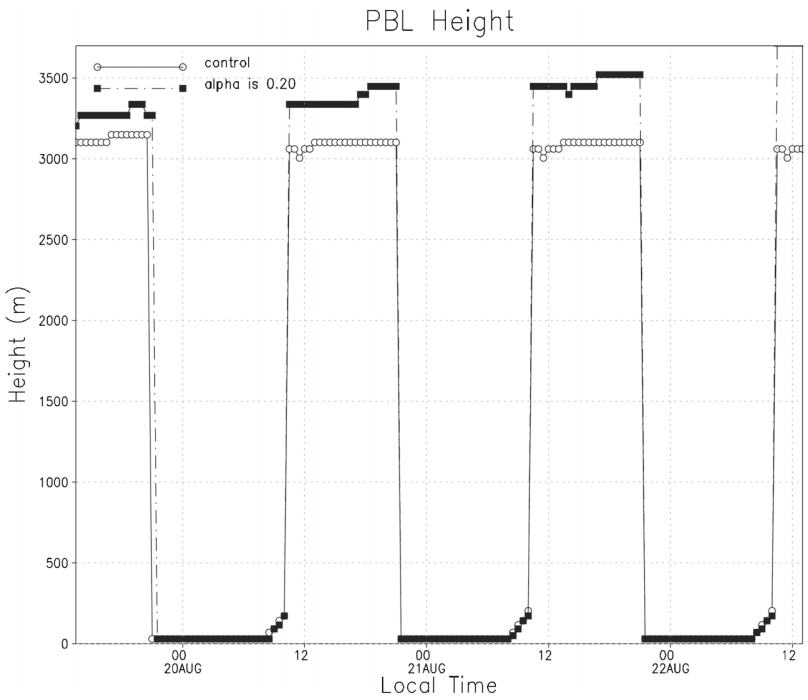

Figure 1. Temporal evolution of the boundary layer height for the enhanced entrainment and control cases.

overshooting thermals to alter the temperature, water vapor mixing ratio, winds, and CO_2 mixing ratios of the boundary layer and the lowest layer of the inversion. The heat flux can be used to define a time rate of change of potential temperature:

$$\frac{\partial \theta}{\partial t} = \frac{\alpha \overline{w' \theta_v'}|_s}{\Delta z}. \tag{2}$$

where Δz is the thickness of the layer. The heat flux across the capping inversion can be used to define a mass flux representative of the amount of mixing between the layers surrounding the interface between the boundary layer and the capping inversion required to produce these temperature changes. This mass flux is given by:

$$M = \frac{\rho \alpha \overline{w' \theta_v'}|_s}{\Delta \theta_v} \tag{3}$$

where ρ is the density of the air and is computed from the total Exner function and ice-liquid potential temperature prognosed by RAMS (Medvigy et al. 2005). This gives the mass flux the units of kg m^{-2} s^{-1}. When multiplied by the specific humidity of the layer, r_v, this becomes a mass flux of water vapor. This can be used to find a time rate of change of the mixing ratio:

$$\frac{\partial r_v}{\partial t} = \frac{\Delta r_v M}{\rho \Delta z}. \tag{4}$$

This induces a drying of the whole boundary layer through turbulent mixing and a moistening of the capping inversion.

This same mass flux can be used to define time rates of change of the different components of the wind vector, TKE, and CO_2 concentration given in the equations below.

$$\frac{\partial u_i}{\partial t} = \frac{\Delta u_i M}{\rho \Delta z} \tag{5}$$

$$\frac{\partial w}{\partial t} = \frac{\Delta w M}{\rho \Delta z} \tag{6}$$

$$\frac{\partial TKE}{\partial t} = \frac{\Delta TKE * M}{\rho \Delta z} \tag{7}$$

$$\frac{\partial C}{\partial t} = \frac{\Delta C * M}{\rho \Delta z} \tag{8}$$

In these equations, u_i represents the two components of the horizontal wind vector. These equations represent the mixing across the overlying capping inversion and introduce negative fluxes of horizontal momentum and CO_2 concentration and positive vertical fluxes of vertical velocity and TKE.

The simulated boundary layer height is diagnosed from the virtual potential temperature profile as the height where the temperature increases by 0.5 K, defining the capping inversion. After the PBL height is determined by this method, the temperature, mixing ratio, wind velocity, TKE, and carbon dioxide concentration tendencies for the layers above and below Z_i are altered by the above equations.

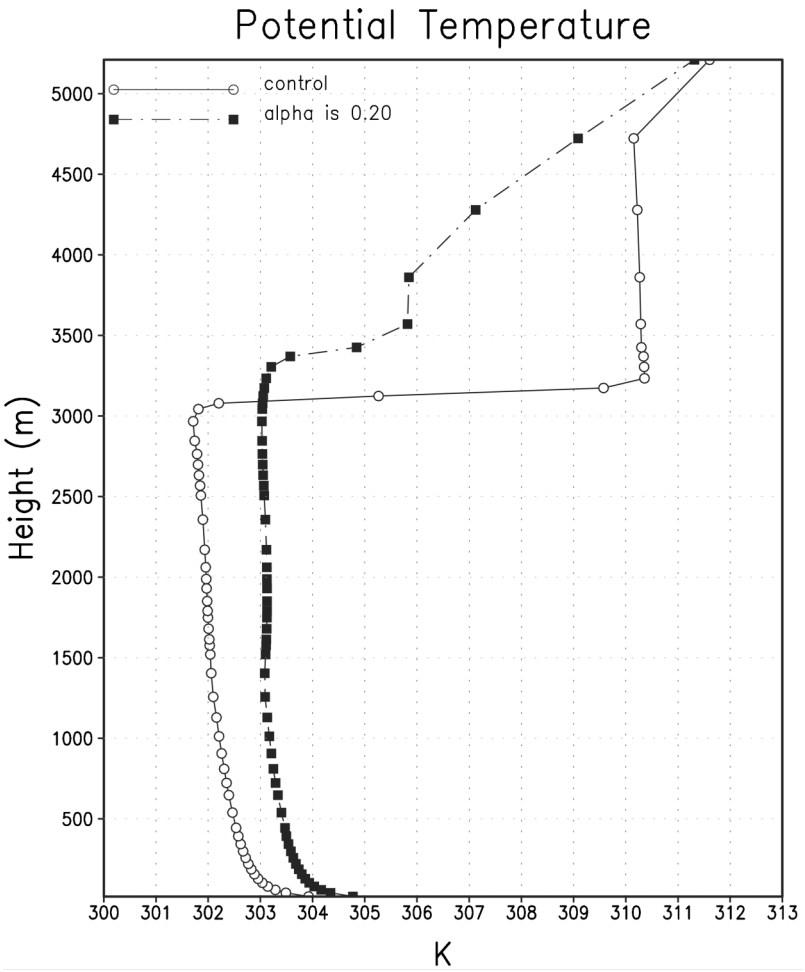

Figure 2. Vertical profile of potential temperature for both the enhanced entrainment and control cases at 13:00 LST on 21 August.

Before the end of the timestep, the seven variables are updated by their respective tendency arrays.

4. Results

a. Physical effects

Inclusion of a parameterization for boundary layer entrainment due to overshooting thermals results in a deeper boundary layer as is evident in Figure 1. It is important to note that the simulated boundary layer is about two times deeper than that typically observed due to the idealized and simplified nature of the model in this case. A residual layer that retains its well-mixed properties throughout the night develops during the evening transition. In the morning, when the sun heats the surface and the nocturnal inversion is broken, the boundary layer quickly grows to the depth of the residual layer. While the morning growth is very rapid once the convective boundary layer reaches the base of the residual layer (Stull 1988) this transition is more rapid in the simplified case than what is typically observed due to little adjustment of the residual layer. The entraining case is the one for which α in the parameterization is given a value of 0.2. The control case does not include the PBL top entrainment parameterization. The greater depth is a product of the input of heat energy from the overlying inversion and the upward transport of turbulent kinetic energy, physically incorporating the lowest levels of the inversion into the boundary layer. The modeled boundary layer is allowed to grow as long as the surface sensible heat flux is positive. Once it becomes negative, an inversion is formed and the boundary layer collapses. The discretized nature of the model does not allow the boundary layer to grow in a smooth way as it would in the physical world. Z_i is limited by the predetermined model levels and can only change when enough energy is present to move from one level to the next.

Figure 2 shows a vertical profile of potential temperature. Throughout the depth of the boundary layer, the entraining case is warmer than the control case by about a degree. However, the inversion is slightly cooler in the entraining case. The combination of a warmer mixed layer and a weaker capping inversion means that it is easier for over-

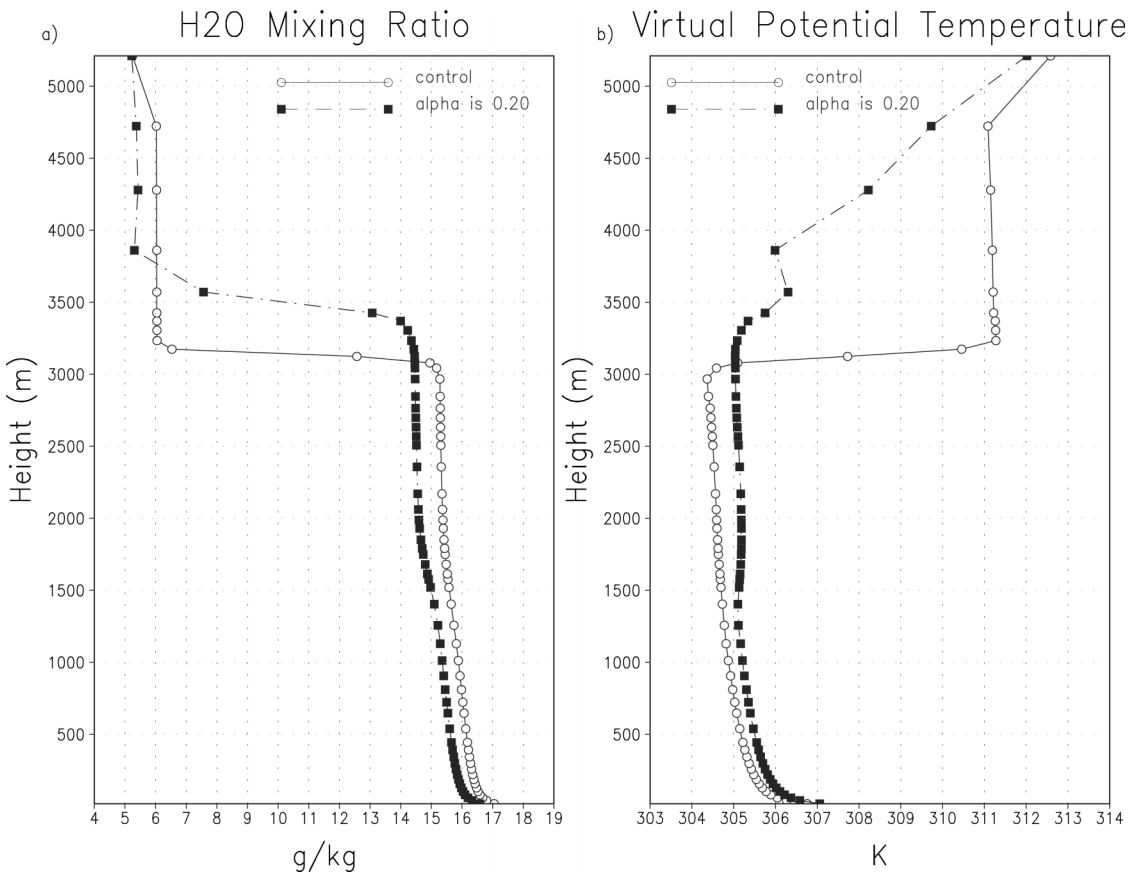

Figure 3. Profile of water vapor mixing ratio (a) and virtual potential temperature (b) for both the enhanced entrainment and control cases at 13:00 LST on 21 August.

shooting thermals to break through the inversion and grow the boundary layer through entrainment. In addition, since the boundary layer is warmer, less surface heating is required to erode the inversion and grow the boundary layer. Turbulent mixing within the boundary layer distributes this warming throughout its depth.

The water vapor mixing ratio profile is also modified by the parameterization (Figure 3a). The upward transport of moisture, carried by the overshooting thermals, results in a drier boundary layer and a moister inversion layer in the entraining case.

The effects of the parameterization on the potential temperature and the water vapor mixing ratio act in opposite directions, since increased water vapor decreases the density of an air mass. Virtual potential temperature (Figure 3b) can be related to potential temperature and water vapor mixing ratio through the equation:

$$\theta_v = \theta(1 + 0.61 r_v) \tag{9}$$

and so demonstrates the combined effect of the parameterization.

The temporal evolution of latent and sensible heat fluxes from the canopy air space (CAS) into the boundary layer is shown in Figures 4a and 4b respectively. The enhanced entrainment case minus the control case is shown in Figure 4c for both sensible and latent heat fluxes. The daytime sensible heat flux is smaller in the entraining case due to the altered conditions that result from the enhanced PBL top entrainment. Since the parameterization is proportional to the surface heat flux, reducing this flux reduces the effects of the thermals.

As was the case for potential temperature and water vapor mixing ratio, the response of PBL top entrainment has opposite impacts on the sensible and latent heat fluxes. The drier boundary layer means that the gradient in water vapor mixing ratio between the boundary layer and the CAS is stronger in the entraining case. The impact of increasing latent heat flux to the total virtual potential temperature flux is to increase it. The larger heat flux then contributes to a larger impact of the parameterization on the heat flux at the top of the boundary layer. The additional moisture from the surface source is then mixed upward by turbulent eddies to moisten the depth of the boundary layer.

b. Physiological effects

The physical modifications to the boundary layer directly impact the vegetation at the surface. The energy budget of the vegetated land surface partitions net downward radi-

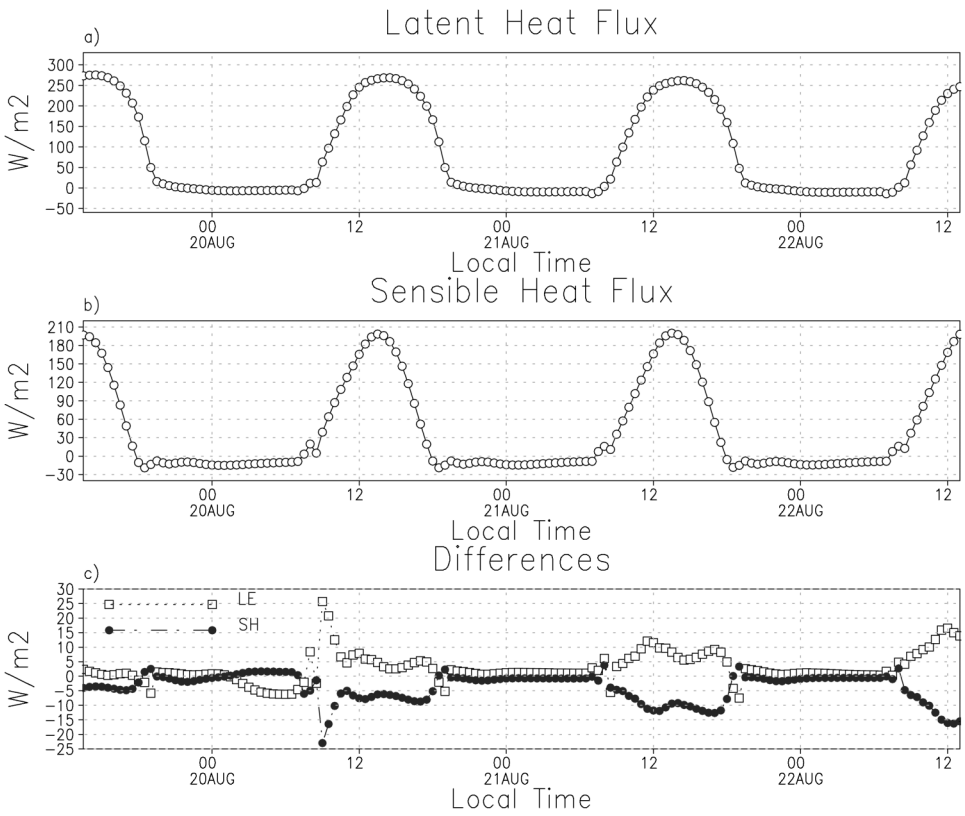

Figure 4. Temporal evolution of the latent (a) and sensible (b) heat fluxes in the lowest atmospheric model level for the control case and the difference (c) given by the enhanced entrainment case minus the control case.

ation into turbulent fluxes of heat and moisture that warm and moisten the atmosphere, plus a smaller heat flux into the soil. The Bowen ratio of sensible to latent heat fluxes is determined by the conductance of plant stomata, which is actively controlled as an evolved response by plants to maximize CO_2 uptake by photosynthesis while minimizing water loss (Ball et al. 1987; Collatz et al. 1991; Bonan et al. 2002). Stomatal conductance (and hence transpiration) is generally greatest when photosynthetic carbon uptake is greatest, the air is nearly saturated with respect to water vapor, and the temperature moderate. The drying influence of entrainment can produce a humidity stress on the plants so that they close their stomata, causing a response in transpiration, the surface energy budget, and photosynthetic rates (Davis et al. 1997).

Stomatal conductance and photosynthesis were calculated iteratively according to enzyme kinetics, diffusion of CO_2 and water vapor, and the Ball-Berry equation (Collatz et al, 1991). Stomatal conductance is directly proportional to the relative humidity at the leaf surface (inside the laminar boundary layer surrounding the leaf), and is adjusted downward by multiplying by nondimensional "stress factors" to account for non-optimal temperatures or insufficient soil moisture (Sellers et al, 1996) (Figure 5).

Simulated stomatal conductance (Figure 6) was reduced during the hottest part of each day due to a combination of slightly reduced humidity and high-temperature stress. Entrainment of dry air into the boundary layer by overshooting thermals is communicated through turbulent mixing, leading to a slightly warmer and drier stomatal microenvironment, and therefore reduced stomatal conductance. Note that despite the slight reduction in stomatal conductance, the simulated sensible heat flux was suppressed and latent heat flux was enhanced in the entraining case due to stronger gradients in the surface layer (Figure 4).

Figure 7 shows the impact of the vegetative stress on the net ecosystem exchange (NEE) of CO_2 (Figures 7a and 7b) and its components. In the morning, warmer temperatures cause the entraining case to have very slightly enhanced uptake of carbon. High-temperature stress and low humidity at mid-day produce less uptake. The NEE at night is very similar between the entraining and control cases with slightly greater respiration in the entraining case due to the warmer surface temperature. Ground respiration is a function of the surface soil temperature and varies with the diurnal cycle of temperature (Figures 7c and 7d). Since the entraining case is warmer throughout the simulation, the ground respiration is larger and more carbon is released into the atmosphere from soil decomposition. Warmer and drier air at mid-day suppresses photosynthetic assimilation (Figures 7e and 7f). The entraining thermals in the simulation thus act indirectly on both components of the net

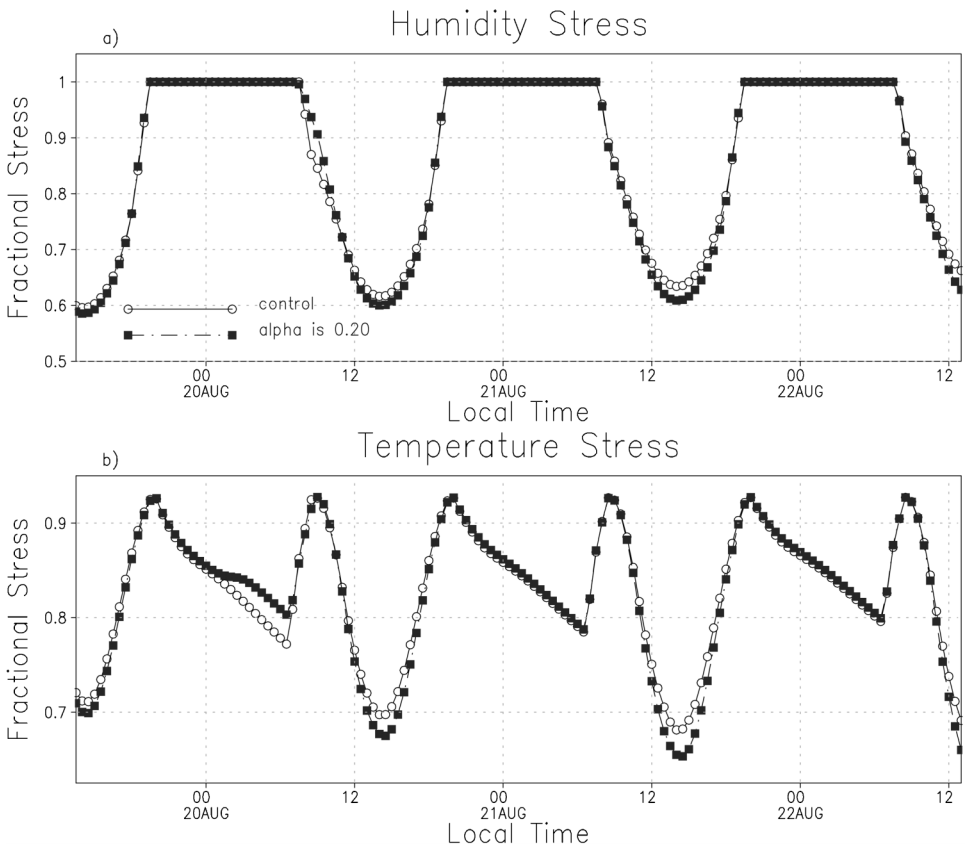

Figure 5. Temporal evolution of vegetative stress factors for the enhanced entrainment and control cases. (a) Humidity stress (b) Temperature stress.

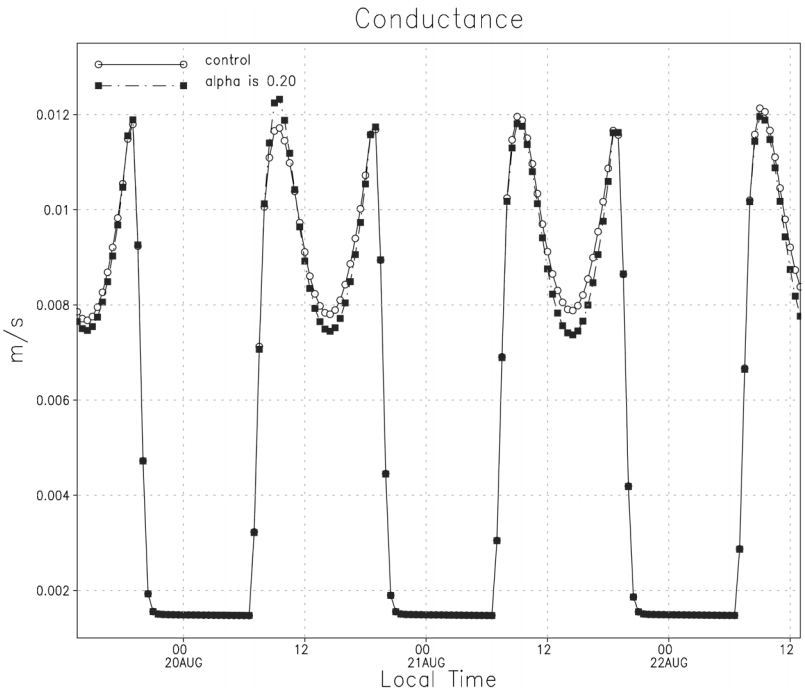

Figure 6. Temporal evolution of conductance for both the enhanced entrainment and control cases.

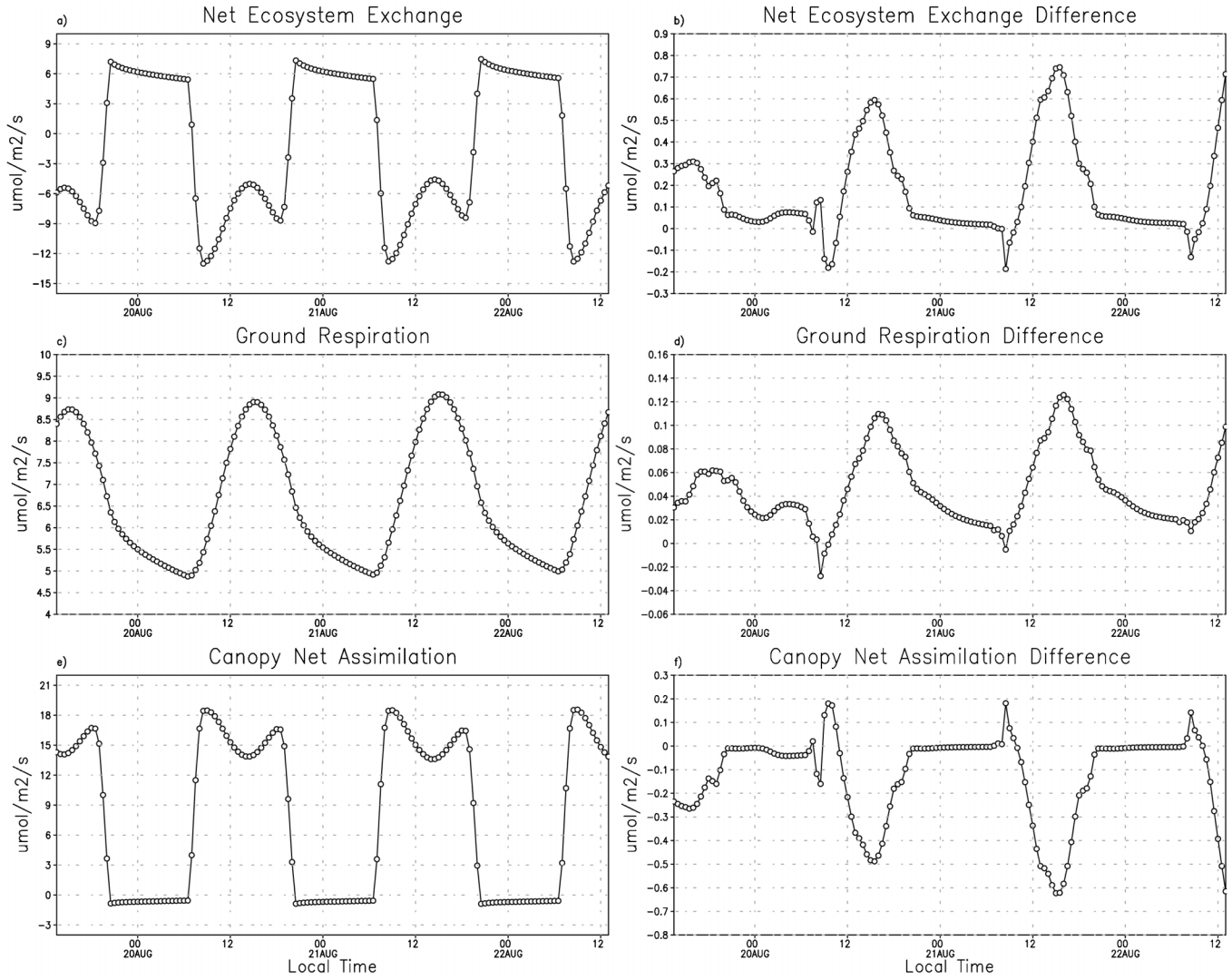

Figure 7. Temporal evolution of NEE (a), ground respiration (c), and canopy net assimilation (e) for the control case and the enhanced entrainment case minus the control case for NEE (b), ground respiration (d), and net assimilation (f).

CO_2 exchange to suppress the drawdown of CO_2 from the PBL through their effects on temperature and moisture.

The overall impact of simulated entrainment on CO_2 in the PBL reflects the modified NEE as well as dilution through the deeper mixed layer and enhanced mixing through the PBL top. Figure 8 shows only the daytime concentration of CO_2 since this study is not concerned with nighttime values. During the day, negative NEE draws down the CO_2 concentration. The daily minimum in CO_2 concentration occurs near sunset, just as the vegetation stops removing carbon from the atmosphere.

CO_2 concentrations in the entraining case are higher than the control due to both the reduced assimilation and the depth of the boundary layer. The dilution effect dominates the increased CO_2 concentrations. As the boundary layer grows, a greater volume of the atmosphere is in contact with the surface and the removal of a given amount of carbon through photosynthesis reduces the CO_2 concentration less.

c. Parameterization magnitude effects

The previous results were obtained by setting the tunable parameter, α, to 0.20, indicating that the entrainment heat flux at the top of the boundary layer was assumed to be 20% of the surface heat flux. The following discussion determines the sensitivity of the system to varying strengths of the parameterization by using values of α between 0.0 and 0.5.

Figure 9 illustrates how potential temperature (Figure 9a), water vapor mixing ratio (Figure 9b), Z_i (Figure 9c), and CO_2 concentration (Figure 19d) in the lowest atmospheric model level vary as functions of α. The values are averaged over 8 hour periods centered on 4 pm (from 12 pm - 8 pm) for the 3 days of 20–22 August. The

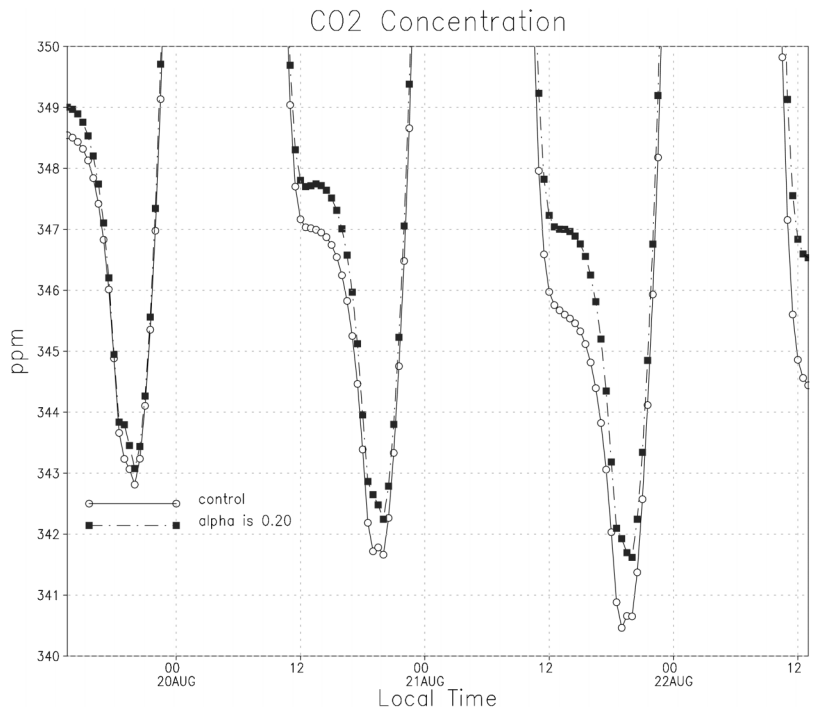

Figure 8. Temporal evolution of carbon dioxide concentration in the lowest atmospheric model level for the enhanced entrainment and control cases.

dashed lines represent the best linear fit to the data and are significant at the 90% level for all four plots. The potential temperature and relative humidity plots are significant at the 97.5% level. The potential temperature nearly linearly increases with α. Neglecting entrainment can result in boundary layer temperature errors that can also affect the assimilation of carbon by plants.

The water vapor mixing ratio generally declines for increasing α. As α increases, overshooting thermals remove water from the boundary layer and transfer it to the overlying inversion. As the boundary layer dries, the moisture gradient between the CAS and the boundary layer increases, producing a greater latent heat flux. The latent heat flux moistens the boundary layer, acting contrary to the overshooting thermals.

The boundary layer height is dependent upon the vertical grid spacing. Energy is needed for Z_i to jump from one level to the next, and greater vertical resolution requires less energy to make a jump, but each jump is smaller. Z_i generally increases with α, indicating that a negative heat flux at the PBL top induces an increase in PBL depth.

Figure 9d shows how CO_2 concentration varies as a function of α. As α increases, so also does the concentration of CO_2. This can be attributed to deeper boundary layers diluting the effect of photosynthetic uptake and increased vegetative stress associated with the warmer and drier conditions of an entrainment heat flux. The dependency of CO_2 concentration with the strength of this entrainment process is important for understanding carbon inversion study results.

5. Conclusions

The effects of PBL top entrainment are important to studies of the carbon budget using modeling. This study examines the impacts of overshooting thermals in an idealized experiment in an attempt to understand the complex interactions between PBL top entrainment, boundary layer processes, and the surface vegetation. Surface fluxes of NEE, sensible and latent heat and CO_2 concentration are sensitive to the magnitude of the entrainment rate through a coupling between these fluxes and those at the PBL top. Increased PBL depth means that uptake of carbon is diluted through a deeper layer, increasing carbon concentrations while the mass and heat fluxes associated with entrainment affect the atmospheric conditions to which the underlying vegetation respond. The altered response, in turn, affects the photosynthetic uptake of carbon thereby increasing the daytime CO_2 concentration even further. Since most observations of CO_2 are performed within the boundary layer, neglect of this process in models such as SiB-RAMS produces a model-observation mismatch and introduces errors into the assumed distribution of sources and sinks.

With this end in mind, the parameterization added to SiB-RAMS introduces a negative sensible heat flux and a positive water vapor flux at the top of the boundary layer and the sensitivity of the surface response was examined.

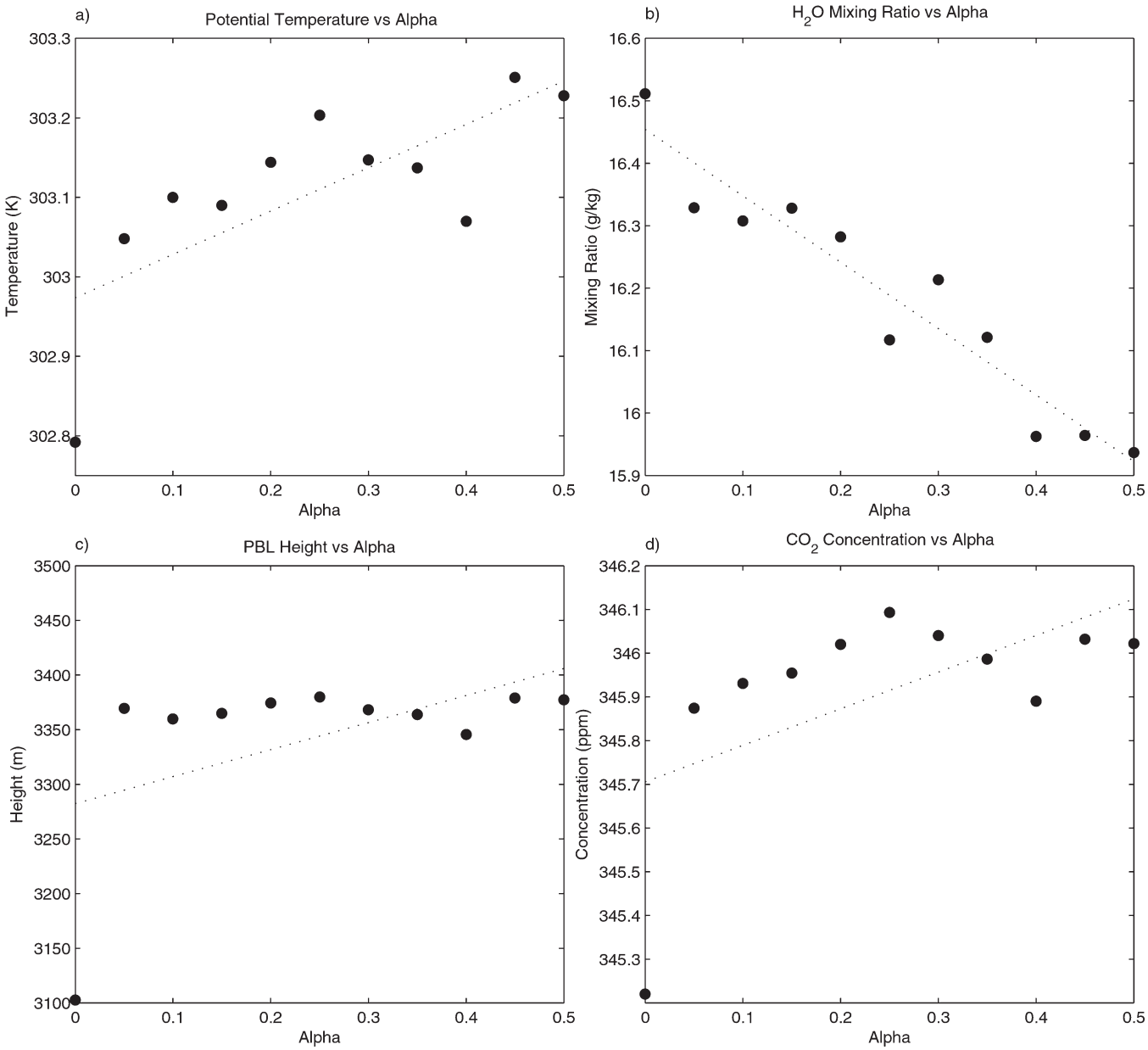

Figure 9. Sensitivity of potential temperature (a), water vapor mixing ratio (b), PBL depth (c), and CO_2 concentration (d) in the lowest model level to α. Values are averaged over an 8 hour period centered on 4 pm for 20–22 August. The dashed lines represent the best linear fit.

The parameterization does induce a warmer, drier boundary layer that affects such characteristics as sensible and latent heat fluxes, wind velocity, and carbon dioxide concentration.

Acknowledgments: The authors are thankful to the three anonymous reviewers for providing many helpful comments that resulted in substantial improvements of the manuscript. This research was supported by National Aeronautics and Space Administration grant NNG05GD15G.

References

André, J. C., De Moor, G., Lacarrère, P., Therry, G., and Du Vachat, R., 1978: Modeling the 24-hour evolution of the mean and turbulent structures of the planetary boundary layer. *J. Atmos. Sci.*, **35**, 1861–1883, doi: 10.1175/1520-0469(1978)035<1861:MTHEOT>2.0.CO;2.

Ayotte, K. W., Sullivan, P. P., Andrén, A., Doney, S. C., Holtslag, A. A. M., Large, W. G., McWilliams, J. C., Moeng, C.-H., Otte, M. J., Tribbia, J. J., and Wyngaard, J. C., 1996: An evaluation of neutral and convective plan-

etary boundary layer parameterizations relative to large eddy simulation. *Bound. –Lay. Meteorol.,* **79**, 131–175, doi: 10.1007/BF00120078.

Ball, J. T., Woodrow, I. E., and Berry, J. A., 1987: A model predicting stomatal conductance and its contribution to the control of photosynthesis under different environmental conditions. Progress in Photosynthesis Research, ed. J. Biggens, 221–224

Beljaars, A. C. M. and Betts, A. K., 1992: Validation of the boundary layer representation in the ECMWF model. ECMWF Seminar Proceedings, 7–11 September 1992, Validation of models over Europe, Vol II, 159–195

Betts, A. K., 1973: Non-precipitating cumulus convection and its parameterization. *Q. J. Roy. Meteor. Soc.*, **99**, 178–196, doi: 10.1002/qj.49709941915.

Bonan, G. B., Lewis, S., Kergoat, L., and Oleson, K. W., 2002: Landscapes as patches of plant functional types: An integrating concept for climate and ecosystem models. *Global Biogeochem. Cycles*, **16(2)**, 1021, doi: 10.1029/2000GB001360.

Carson, D. J., 1973: The development of a dry inversion-capped convectively unstable boundary layer. *Q. J. Roy. Meteor. Soc.*, **99**, 450–467, doi: 10.1002/qj.49709942105.

Cohn, S. A. and Angevine, W. M., 2000: Boundary layer height and entrainment zone thickness measured by lidars and wind-profiling radars. *J. Appl. Meteorol.*, **39**, 1233–1247, doi: 10.1175/1520-0450(2000)039<1233:BLHAEZ>2.0.CO;2.

Collatz, G. J., Ball, J. T., Grivet, C., and Berry, J. A., 1991: Physiological and environmental regulation of stomatal conductance, photosynthesis and transpiration: A model that includes a laminar boundary layer. *Agr. Forest Meteorol.*, **54**, 107–136, doi: 10.1016/0168-1923(91)90002-8.

Corbin, K. D., Denning, A. S., Lu, L., Wang, J.-W., and Baker, I. T., 2008: Possible representation errors in inversions of satellite CO_2 retrieval. *J. Geophys. Res.*, **113**, D02301, doi: 10.1029/2007JD008716.

Cotton, W. R., Pielke, Sr. R. A., Walko, R. L., Liston, G. E., Tremback, C. J., Jiang, H., McAnelly, R. L., Harrington, J. Y., Nicholls, M. E., Carrio, G. G., and McFadden, J. P., 2003: RAMS 2001: Current status and future directions. *Meteorol. Atmos. Phys.*, **82**, 5–29, doi: 10.1007/s00703-001-0584-9.

Davis, K. J., Lenschow, D. H., Oncley, S. P., Kiemle, C., Ehret, G., Giez, A., and Mann, J., 1997: Role of entrainment in surface-atmosphere interactions over the boreal forest. *J. Geophys. Res.*, **102**, D24, 29219–29230, doi: 10.1029/97JD02236.

Deardorff, J. W., 1974: Three-dimensional numerical study of the height and mean structure of a heated planetary boundary layer. *Bound -Lay Meteorol.*, **7**, 81–106, doi: 10.1007/BF00224974.

Denning, A. S., Fung, I. Y., and Randall, D. A., 1995: Latitudinal gradient of atmospheric CO_2 due to seasonal exchange with land biota. *Nature*, **376**, 240–243, doi: 10.1038/376240a0.

Denning, A. S., Collatz, J. G., Zhang, C., Randall, D. A., Berry, J. A., Sellers, P. J., Colello, G. D., and D.A. Dazlich, D. A. 1996a: Simulations of terrestrial carbon metabolism and atmospheric CO_2 in a general circulation model. Part 1: Surface carbon fluxes. *Tellus*, **48B**, 521–542, doi: 10.1034/j.1600-0889.1996.t01-2-00009.x.

Denning, A. S., Randall, D. A., Collatz, G. J., and Sellers, P. J., 1996b: Simulations of terrestrial carbon metabolism and atmospheric CO_2 in a general circulation model. Part 2: Spatial and temporal variations of atmospheric CO_2. *Tellus*, **48B**, 543–567, doi: 10.1034/j.1600-0889.1996.t01-1-00010.x.

Denning, A. S., Takahashi, T., and Friedlingstein, P., 1999: Can a strong atmospheric CO_2 rectifier effect be reconciled with a ''reasonable carbon budget? *Tellus*, **51B**, 249–253, doi: 10.1034/j.1600-0889.1999.t01-1-00010.x.

Denning, A. S., Nicholls, M., Prihodko, L., Baker, I., Vidale, P.-L., Davis, K., and Bakwin, P., 2003: Simulated variations in atmospheric CO_2 over a Wisconsin forest using a coupled ecosystem-atmosphere model. *Glob. Change Biol.*, **9**, 1241–1250, doi: 10.1046/j.1365-2486.2003.00613.x.

Denning, A. S., Zhang, N., Yi, C., Branson, M., Davis, K., Kleist, J., and Bakwin, P., 2008: Evaluation of modeled atmospheric boundary layer depth at the WLEF tower. *Agr. Forest Meteorol.*, **148**, 206–215, doi: 10.1016/j.agrformet.2007.08.012.

Farquhar, G. D., Caemmerer, S. V., and Berry, J. A., 1980: A biochemical-model of photosynthetic CO_2 assimilation in leaves of C-3 species. *Planta*, **149**, 78–90, doi: 10.1007/BF00386231.

Freitas, S. R., Longo, K., Silva Dias, M., Silva Dias, P., Chatfield, R., Fazenda, Á., and Rodrigues, L. F., 2006: The coupled aerosol and tracer transport model to the Brazilian developments on the Regional Atmospheric Modeling System: Validation using direct and remote sensing observations. International Conference on Southern Hemisphere Meteorology and Oceanography (ICSHMO), 8., 101–107. CD-ROM. ISBN 85-17-00023-4

Gerbig, C., Lin, J. C., Wofsy, S. C., Daube, B. C., Andrews, A. E., Stephens, B. B., Bakwin, P. S., and Grainger, C. A., 2003a: Toward constraining regional-scale fluxes of CO_2 with atmospheric observations over a continent: 1. Observed spatial variability from airborne platforms. *J. Geophys. Res.*, **108**, D24, doi: 10.1029/2002JD003018.

Gerbig, C., Lin, J. C., Wofsy, S. C., Daube, B. C., Andrews, A. E., Stephens, B. B., Bakwin, P. S., and Grainger, C. A., 2003b: Toward constraining regional-scale fluxes of CO_2 with atmospheric observations over a continent: 2. Analysis of COBRA data using a receptor-oriented framework. *J. Geophys. Res.*, **108**, D24, doi: 10.1029/2002JD003018.

Gerbig, C., Körner, S., and Lin, J. C., 2008: Vertical mixing in atmospheric tracer transport models: Error characterization and propagation. *Atmos. Chem. Phys.*, **8**, 591–602

Gurney, K. R., Law, R. M., Denning, A. S., Rayner, P. J., Baker, D., Bousquet, P., Bruhwiler, L., Chen, Y.-H., Ciais, P., Fan, S., Fung, I. Y., Gloor, M., Heimann, M., Higuchi, K., John, J., Maki, T., Maksyutov, S., Masarie, K., Peylin, P., Prather, M., Pak, B. C., Randerson, J., Sarmiento, J., Taguchi, S., Takahashi, T., and Yuen, C.-W., 2002: Towards robust regional estimates of CO_2 sources and sinks using atmospheric transport models. *Nature*, **415**, 626–630, doi: 10.1038/415626a.

Medvigy, D., Moorcroft, P. R., Avissar, R., and Walko, R. L., 2005: Mass conservation and atmospheric dynamics in the Regional Atmospheric Modeling System (RAMS). *Environ. Fluid Mech.*, **5**, 109–134, doi: 10.1007/s10652-005-5275-5.

Mellor, G. L. and Yamada, T., 1982: Development of a turbulence closure model for geophysical fluid problems. *Rev. Geophys.*, **20**, 851–875, doi: 10.1029/RG020i004p00851.

Nicholls, M. E., Denning, A. S., Prihodko, L., Vidale, P.-L., Baker, I., Davis, K., and Bakwin, P., 2004: A multiple-scale simulation of variations in atmospheric carbon dioxide using a coupled-biosphere-atmospheric model. *J. Geophys. Res.*, **109**, D18117, doi: 10.1029/2003JD004482.

Pielke, R. A., 1974: A three-dimensional numerical model of the sea breezes over south Florida. *Mon. Weather Rev.*, **102**, 115–139, doi: 10.1175/1520-0493(1974)102<0115:ATDNMO>2.0.CO;2.

Pielke, R. A., 1991: Overlooked scientific issues in assessing hypothesized greenhouse gas warming. *Environ. Software*, **6**, 100–107, doi: 10.1016/0266-9838(91)90035-O.

Pielke, R. A., Cotton, W. R., Walko, R. L., Tremback, C. J., Lyons, W. A., Grasso, L. D., Nicholls, M. E., Moran, M. D., Wesley, D. A., Lee, T. J., and Copeland, J. H., 1992: A comprehensive meteorological modeling system RAMS. *Meteorol. Atmos. Phys.*, **49**, 69–91, doi: 10.1007/BF01025401.

Rayment, R. and Readings, C. J., 1974: A case study of the structure and energetics of an inversion. *Q. J. Roy. Meteorol. Soc.*, **100**, 221–233, doi: 10.1002/qj.49710042409.

Sayler, B. J. and Breidenthal, R. E., 1998: Laboratory simulations of radiatively induced entrainment in stratiform clouds. *J. Geophys. Res.*, **103**, 8827–8837, doi: 10.1029/98JD00344.

Sellers, P. J., Mintz, Y., Sud, Y. C., and Dalcher, A., 1986: A simple biosphere model (SiB) for use within general circulation models. *J. Atmos. Sci.*, **43**, 505–531, doi: 10.1175/1520-0469(1986)043<0505:ASBMFU>2.0.CO;2.

Sellers, P. J., Randall, D. A., Collatz, G. J., Berry, J. A., Field, C. B., Dazlich, D. A., Zhang, C., Collelo, G. D., Bounoua, L., 1996: A revised land surface parameterization (SiB2) for atmospheric GCMs, Part 1: Model formulation. *J. Climate*, **9**, 676–705, doi: 10.1175/1520-0442(1996)009<0676:ARLSPF>2.0.CO;2.

Sullivan, P. P., Moeng, C.-H., Stevens, B., Lenschow, D. H., and Mayer, S. D., 1998: Structure of the entrainment zone capping the convective atmospheric boundary layer. *J. Atmos. Sci.*, **55**, 3042–3064, doi: 10.1175/1520-0469(1998)055<3042:SOTEZC>2.0.CO;2.

Stevens, D. E. and Bretherton, C. S., 1999: Effects of resolution on the simulation of stratocumulus entrainment. *Q. J. Roy. Meteorol. Soc.*, **125**, 425–439, doi: 10.1002/qj.49712555403.

Stull, R. B., 1976: The energetics of entrainment across a density interface. *J. Atmos. Sci.*, **33**, 1260–1267, doi: 10.1175/1520-0469(1976)033<1260:TEOEAD>2.0.CO;2.

Stull, R. B., 1988: An introduction to boundary layer meteorology. Kluwer Academic Publishers, Norwell, MA. 666 pp

Tripoli, G. J. and Cotton, W. R., 1982: The Colorado State University thee-dimensional cloud/mesoscale model – 1982. Part I: General theoretical framework and sensitivity experiments. *J. Rech. Atmos.*, **16**, 185–220

Walko, R. L., Tremback, C. J., Panetta, J., Freitas, S., and Fazenda, A. L., 2002: RAMS Regional Atmospheric Modeling System version 5.0 model input namelist parameters. http://www.cptec.inpe.br/brams/input_namelist.shtml, access 8 Dec 2007

Wang, J.-W., Denning, A. S., Lu, L., Baker, I. T., Corbin, K. D., and Davis, K. J., 2007: Observations and simulations of synoptic, regional, and local variations in atmospheric CO_2. *J. Geophys. Res.*, **112**, D04108, doi: 10.1029/2006JD007410.

Willis, G. E. and Deardorff, J. W., 1974: A laboratory model of the unstable planetary boundary layer. *J. Atmos. Sci.*, **31**, 1297–1307, doi: 10.1175/1520-0469(1974)031<1297:ALMOTU>2.0.CO;2.

Yi, C., Davis, K. J., Berger, B. W., and Bakwin, P. S., 2001: Long-term observations of the dynamics of the continental planetary boundary layer. *J. Atmos. Sci.*, **58**, 1288–1299, doi: 10.1175/1520-0469(2001)058<1288:LTOOTD>2.0.CO;2.

Yi, C., Davis, K. J., Bakwin, P. S., Denning, A. S., Zhang, N., Desai, A., Lin, J. C., and Gerbig, C., 2004: Observed covariance between ecosystem carbon exchange and atmospheric boundary layer dynamics at a site in northern Wisconsin. *J. Geophys. Res.*, **109**, D08302, doi: 10.1029/2003JD004164.

Zhang, N., 2002: Observations and simulations of the planetary boundary layer at a tall tower in northern Wisconsin. Master's thesis, Colorado State University, Department of Atmospheric Science, Fort Collins, CO 80523, 71 pp

Zupanski, D., Denning, A. S., Uliasz, M., Zupanski, M., Schuh, A. E., Rayner, P. J., Peters, W., and Corbin, K., 2007: Carbon flux bias estimation employing Maximum Likelihood Ensemble Filter (MLEF). *J. Geophys. Res.*, **112**, D17107, doi: 10.1029/2006JD008371.